6th International Conference on NDE in Relation to Structural Integrity for Nuclear and Pressurized Components
October 2007, Budapest, Hungary
For more papers of this publication click: www.ndt.net/search/docs.php3?MainSource=70

Modelling II

# Development of Eddy Current Simulation Features within CIVA for the Analysis of Steam Generator Tubing Inspection Safety Issues

G. Pichenot, C. Reboud: CEA LIST-SYSSC, France ; T. Sollier, G. Cattiaux: IRSN, France;

## ABSTRACT

The assessment of Steam Generator (SG) tubes integrity is a challenging task with respect to the numerous degradation mechanisms observed worldwide and to the number of tubes in service. In the framework of extended cycles and optimization of their maintenance programs, utilities may revise their technical specifications for SG inspections. These revisions and other current SG safety related issues such as Tube Support Plate (TSP) blockage have to be evaluated by the safety authorities.

IRSN carries out research and analysis on the risk related to radioactivity for the French Safety Authority (ASN). Since many years, IRSN has contributed to the development of simulation tools for the evaluation and expertise of Non-Destructive Testing techniques used by the nuclear industry. These developments, among others from various contributors (industries, research institutes, academics) belonging to diverse industrial branches (nuclear, aeronautics, automotive, metallurgy …) have been appended to the CIVA NDT platform developed by CEA.

In this paper, the main features of CIVA for SG tube inspection are reviewed and commented through typical applications. The bobbin coil inspection configuration is presented in detail. The bobbin coil response to longitudinal notches, transversal notches and volumetric flaws such as flat bottom holes or loss of material can be simulated. The effect of possible probe eccentricity on probe sensitivity might also be assessed. Those simplified configurations might be used to model SG tube degradation mechanisms like Stress Corrosion Cracking (SCC) and, to a certain extent, wear. Although great care has to be taken to extrapolate simplified modeled degradations to realistic industrial configurations, simulation gives valuable information for overall estimation of the probe performances.

For quantitative assessment, the validation of the simulation tools is a key point thus great care has been taken for the comparison between numerical results and experimental data on a set of artificial flaws. The validation approach and the conclusions are presented.

## INTRODUCTION

Health monitoring of Steam Generator (SG) tubes using non-destructive techniques (NDT) like eddy current testing (ECT) constitutes a big stake due to the great number of degradations observed in industrial installations. Typical flaws affecting these tubes are longitudinal or transverse cracks due to the sensitivity of the Nickel-based alloy 600 to stress corrosion cracking. Simulation tools provide important information about flaws detection and NDT devices improvement.

The French Atomic Commission (CEA) has developed for years semi-analytical models dedicated to ECT. These simulations tools, which are proposed in the CIVA software developed by CEA, provide fast and accurate results in the case of canonical geometries. IRSN carries out research and analysis on nuclear safety issues for the French Safety Authority (ASN). IRSN uses the CIVA software for ECT simulation and funds specific studies carried out by CEA.

This paper is organised as follows: the semi-analytical modeling approach used in CIVA is briefly introduced in the first part, and experimental validation results for bobbin coil and rotating probes testing SG tubes are given. In the second part, results of a specific study concerning the influence of some perturbation parameters are presented. Finally, new CIVA tools dedicated to the management of simulations and the study of parameters variations are introduced.

## MODELING OF ECT CONFIGURATIONS INVOLVING STEAM GENERATOR TUBES IN CIVA

Semi-analytical models developed in the CIVA platform use the Volume Integral Method (VIM) based on Green's formalism [1]. The main advantages of this approach are its great accuracy, its speed, since a complete cartography is achieved with CIVA in less than an hour for a 3D ECT configuration, and the few number of numerical parameters required in the configuration description. These numerical parameters are the number of cells used to mesh the flaw and ferrite cores of the probe if any. This last point makes CIVA easier to use than purely numerical simulation tools for non-specialists in numerical analysis.

### Introduction to the VIM approach

Let us consider an infinite and non-magnetic SG tube tested with a bobbin coil. The keystone of the modeling approach consists in the solution of an integral equation [2], governing the interaction between the flaw and the primary electric field emitted by the probe in the volume containing the flaw. This equation can be written considering volume current densities:

$$\mathbf{J}(\mathbf{r}) = \mathbf{J}_0(\mathbf{r}) + j\,\omega\,\mu_0\,\sigma_0\,f(\mathbf{r})\int_{\Omega}\mathbf{G}(\mathbf{r},\mathbf{r}')\cdot\mathbf{J}(\mathbf{r}')\,\mathrm{d}\mathbf{r}', \qquad (1)$$

where $\Omega$ is the volume of the flaw, $\omega$ is the angular frequency, $\mu_0 = 4\pi.10^{-7}$, $\mathbf{G}$ is a dyadic Green's function, $\sigma_0$ is the tube conductivity, $\mathbf{J}_0$ is an exciting term due to the probe and the function $f(\mathbf{r})$, defined by the relation

$$f(\mathbf{r}) = \frac{\sigma_0 - \sigma(\mathbf{r})}{\sigma_0}, \qquad (2)$$

represents the conductivity contrast between the flawed region, which conductivity is $\sigma(\mathbf{r})$, and the unflawed region of conductivity $\sigma_0$. The unknown $\mathbf{J}$ of this equation is a fictitious current density defined in $\Omega$ and is determined using the Method of Moments [3].

In order to solve equation (1), the excitation term $\mathbf{J}_0$ has to be calculated first. This term is obtained from the calculation of the primary electric field emitted by the probe in the region $\Omega$. Depending on the probe's configuration, this electric field is calculated using Green's dyads, in the case of an off-centre bobbin coil [4] for instance, or Dodd and Deeds solutions in the case of a centred bobbin coil. Once the fictitious current density $\mathbf{J}$ has been calculated, ECT output signals are obtained using the reciprocity principle [5].

This modeling approach has been validated with experimental data in the case of several industrial applications. Results presented hereafter concern SG tubes.

### Case of ECT with a bobbin coil

The example illustrated in figure 1 deals with the inspection at two different frequencies of a Steam Generator tube made of Inconel ($\sigma$= 1 MS/m, $\mu_r$ = 1) affected by a transverse flaw, using a bobbin coil made of two coils operating in differential mode. The detailed characteristics of the tube, of the probe and the flaw are given in figure 1. The scanning is performed along the axis of the tube, and simulation results are compared with experimental data in the impedance plane. A calibration procedure is applied using a through-wall cylindrical hole: once the simulation of this calibration flaw has been performed, coefficients are applied in order to fit the experimental data in terms of maximal amplitude and related phase. Those coefficients are therefore applied for any other flaws simulation. One may observe that for both frequencies simulated and experimental results agree quite well, the discrepancy in amplitude and phase being, respectively, lower than 5% in amplitude and 2.5° in phase.

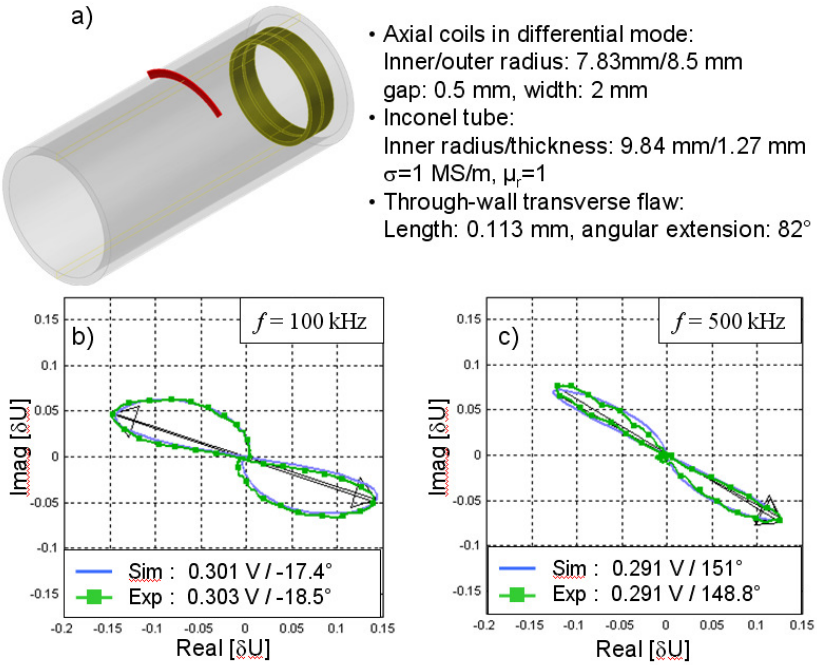


Figure 1 - Experimental and simulated ECT inspection of a transverse flaw with a bobbin coil: a) Configuration description, b) Inspection at $f$ = 100 kHz, c) Inspection at $f$ = 500 kHz.

Another inspection simulation has been carried out and compared to experimental data, using the same probe and the same tube, with a longitudinal flaw (see dimensions on figure 2). Here again, one may observe that for both frequencies simulated results and experimental data agree well, although experimental data exhibits some noise (especially at the frequency of 500 kHz, which is less favourable than lower frequencies for the detection of this external flaw). However, in spite of this noise, the agreement in amplitude and phase is better than 5% and 5°, respectively.

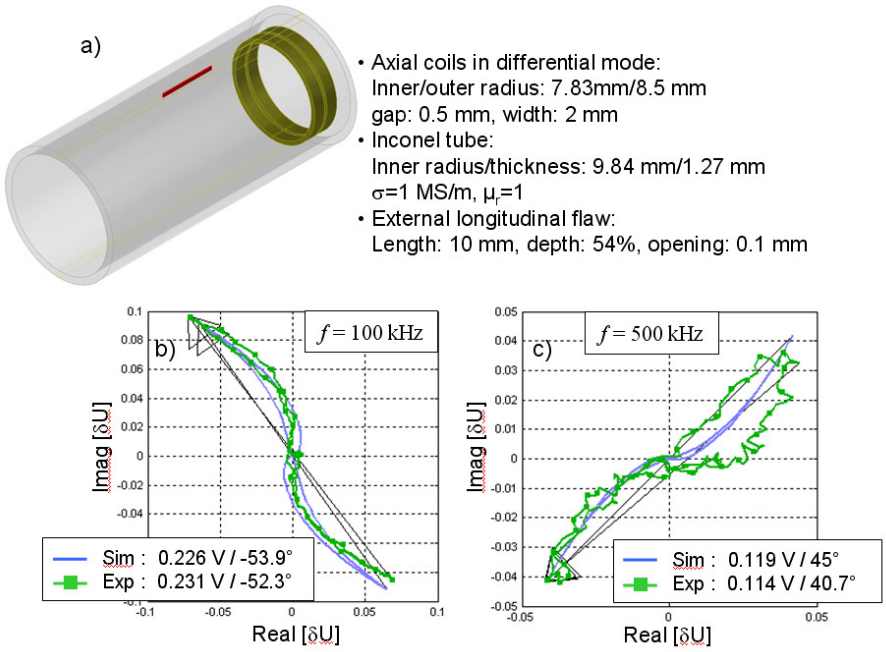


Figure 2 - Experimental and simulated ECT inspection of a longitudinal flaw with a bobbin coil: a) Description of the configuration, b) Inspection at $f$ = 100 kHz, c) Inspection at $f$ = 500 kHz.

The influence of probe eccentricity may also be simulated, as illustrated on the figure below, using two different inspection configurations for a 40% external groove: the first configuration corresponds to a centred probe (as used in the previous experimental validation examples) while, in the second configuration, the axis of the probe has been shifted by 1mm. One may observe that the flaw signal is somewhat increased for the off-centred probe's case.

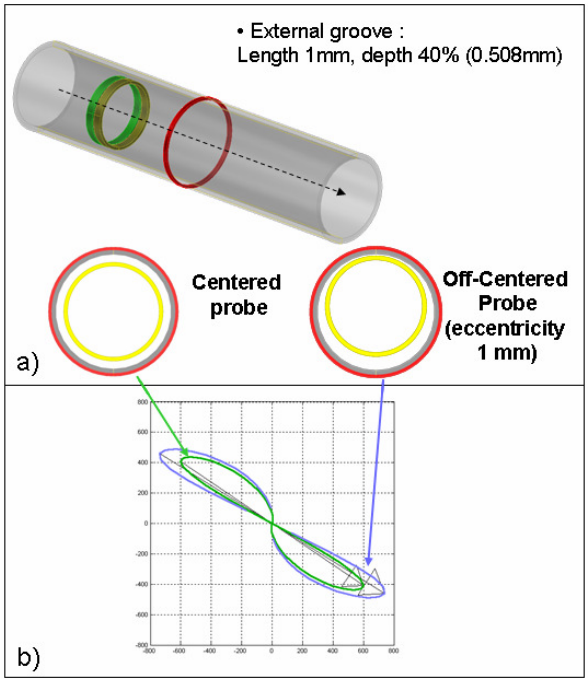


Figure 3 - Simulation of the influence of the probe's alignment over the flaw response:
a) Description of the configuration, b) Simulated results at $f$ = 500 kHz.

**Case of ECT with a rotating probe**

The simulation of an EC rotating probe inspection has been developed in CIVA, in order to deal with probes used for SG tubes inspection, as displayed in figure 4. This rotating probe contains two different sensors that are designed to detect transverse and longitudinal flaws, respectively. Some coils composing these sensors contain ferrite cores.

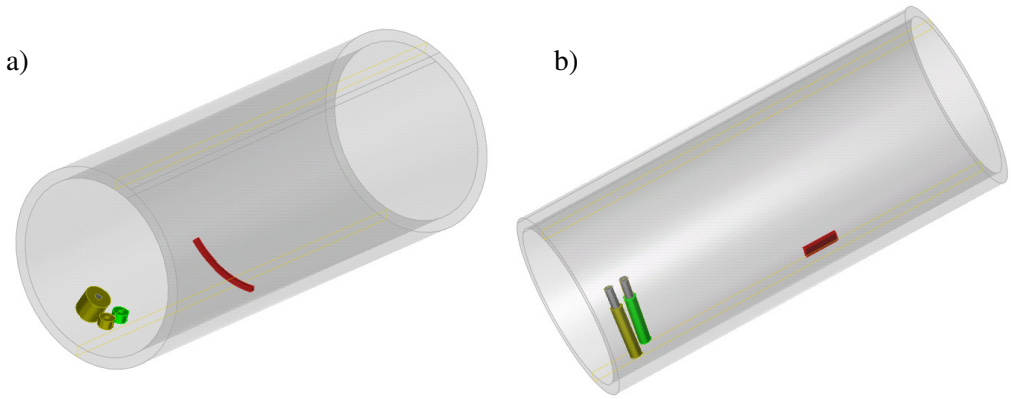


Figure 4 - Schematic illustration of two sensors included in a rotating probe.
a) The emitting coil contains a ferrite core and the receivers operate in differential mode.
b) The two identical coils with a ferrite core are emitting and are receiving in differential mode.

In order to handle such probes, a modeling approach has been used (and successfully validated): as the probes dimensions are relatively small with respect to the tube, one may consider that the specimen may be seen as a plane. Therefore, the probes arrangement (distance between the transmitter and receivers) is projected on the "unwrapped" tube, and the calculation is made using the semi-analytical kernels already developed and validated for planar cases.

## SPECIFIC STUDY CARRIED OUT IN PARTNERSHIP WITH IRSN

Many perturbations may decrease the performance of an ECT method for the flaw detection. Some of them may be studied in simulation. The aim of the study presented thereafter is to have a better understanding of the influence of two particular sets of parameters in the case of the ECT of SG tubes with the sensor described in figure 4 a).

### Effect of the coils positioning

In the first part of the study, the effect of the gap $d_1$ separating the emitting coil and the receiving coil, and the effect of the gap $d_2$ separating the receiving coils, as shown in figure 5, has been estimated in simulation.

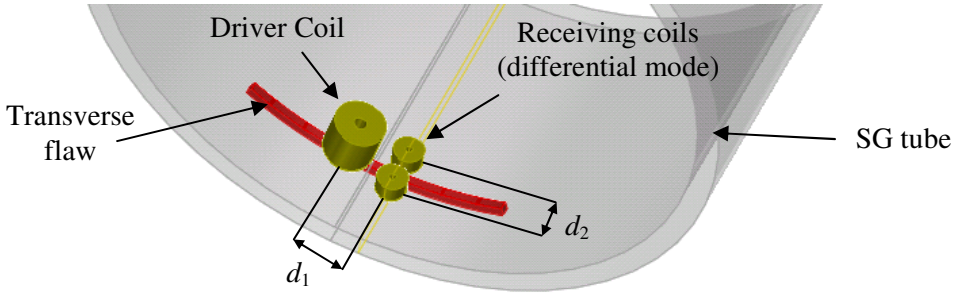


Figure 5 - Definition of distances $d_1$ and $d_2$ for the study of flaw detection in SG tubes using a rotating probe for transversal flaw detection.

When considering an equivalent ECT configuration in a plane geometry, nominal values of these two gaps are $d_{10}$ and $d_{20}$. Simulations were carried out considering combinations of variations of $d_1$ and $d_2$, given in table 1, around these nominal values. Variations considered here are limited to 0.3 mm. For each couple of values ($d_1$,$d_2$), four ECT configurations were simulated (see figure 6). Apart from $d_1$ and $d_2$, geometrical characteristics of the SG tube and the sensor are the same as in the previous section. All flaws dimension along the axis of the tube is 0.1 mm, and simulations are carried out at the frequency of 600 kHz.

| | | | | | | |
|---|---|---|---|---|---|---|
| $d_{10}$-0.3 mm | $d_{10}$-0.2 mm | $d_{10}$-0.1mm | **$d_{10}$** | $d_{10}$+0.1 mm | $d_{10}$+0.2 mm | $d_{10}$+0.3 mm |
| $d_{20}$-0.3 mm | $d_{20}$-0.2 mm | $d_{20}$-0.1mm | **$d_{20}$** | $d_{20}$+0.1 mm | $d_{20}$+0.2 mm | $d_{20}$+0.3 mm |

Table 1 - Variations of the gaps $d_1$ and $d_2$ considered in simulation, which correspond to small variations around the nominal values $d_{10}$ and $d_{20}$.

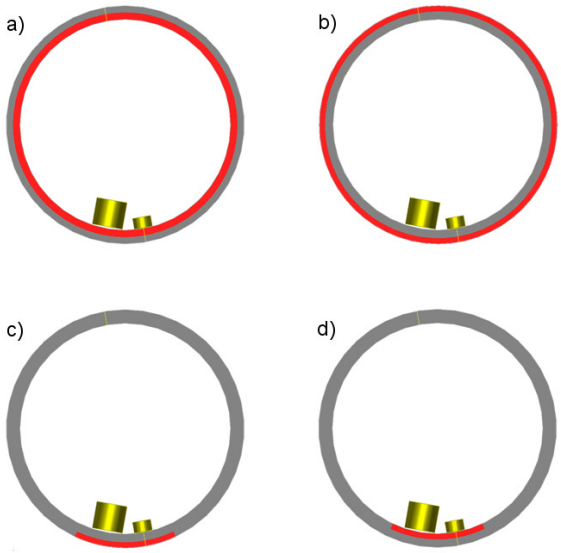


Figure 6 - ECT configurations simulated for the study of the influence of gaps $d_1$ and $d_2$. a) Internal groove with a depth of 50% (*i.e.* 0.635 mm), used for calibration. b) External groove with a depth of 40% (*i.e.* 0.508 mm). c) External transverse notch with a depth of 40% and an angular extension of 50°. d) Internal transverse notch with a depth of 40% and an angular extension of 50°.

After the application of the calibration step, defined for the flaw shown on figure 2 a), each cartography of the imaginary part of the ECT signal (corresponding to the Y channel) has been post-processed outside of the CIVA software in order to take into account the helical motion of the rotating probe. The variation □Y, corresponding to the difference between the maximal and the minimal values of the Y channel, is compared for each couple $(d_1,d_2)$ to its nominal value $\square Y_0$ corresponding to the case $(d_1,d_2) = (d_{10},d_{20})$. Comparisons carried out with the different set of parameters are summarized in table 2. This table show that for the external groove, the external and the internal notches, the detection value □Y is modified in reasonable ranges considering nominal values $\square Y_0$ and detection criteria imposed by the industrial NDT procedure.

| External groove (mV) | External notch (mV) | Internal notch (mV) |
|---|---|---|
| $-19 \leq \square Y_0 - \square Y \leq 21$ | $-22 \leq \square Y_0 - \square Y \leq 23$ | $-18 \leq \square Y_0 - \square Y \leq 20$ |
| Relative variation | Relative variation | Relative variation |
| $\lvert\Delta Y_0 - \Delta Y\rvert / \lvert\Delta Y_0\rvert \leq 17\%$ | $\lvert\Delta Y_0 - \Delta Y\rvert / \lvert\Delta Y_0\rvert \leq 18\%$ | $\lvert\Delta Y_0 - \Delta Y\rvert / \lvert\Delta Y_0\rvert \leq 12\%$ |

Table 2 - Variation ranges of ΔY obtained in simulation with respect to the nominal value $\Delta Y_0$, for considering variations of $(d_1,d_2)$ described in table 1.

**Effect of a variation of the tube geometry**

In the second part of the study, we have been interested in effects consecutive to a variation of the tube geometry, and more specifically a slight ovality of the tube. In this study, the maximal out-of-roundness, defined as the difference between the maximal and the minimal radii of the tube, is taken as 4% of the nominal value (9.84 mm) of SG tubes.

In the case of the ECT sensor described in the previous section, the rigid shape of the probe's support is pushed toward the internal tube's wall by a spring. If the tube's out-of-roundness is different from zero, then some particular lift-off will appear for each coil, as one can see in figure 7. The same lift-off appears for the receiving coils, but another one appears for the emitting coil. These two lift-offs, calculated for a relative out-of-roundness of 4%, are plotted versus the probe's angular position

in figure 8. Although simulations have been carried out considering perfectly cylindrical tubes, the effect of the ovality is taken into account by using these lift-offs when positioning the probe.

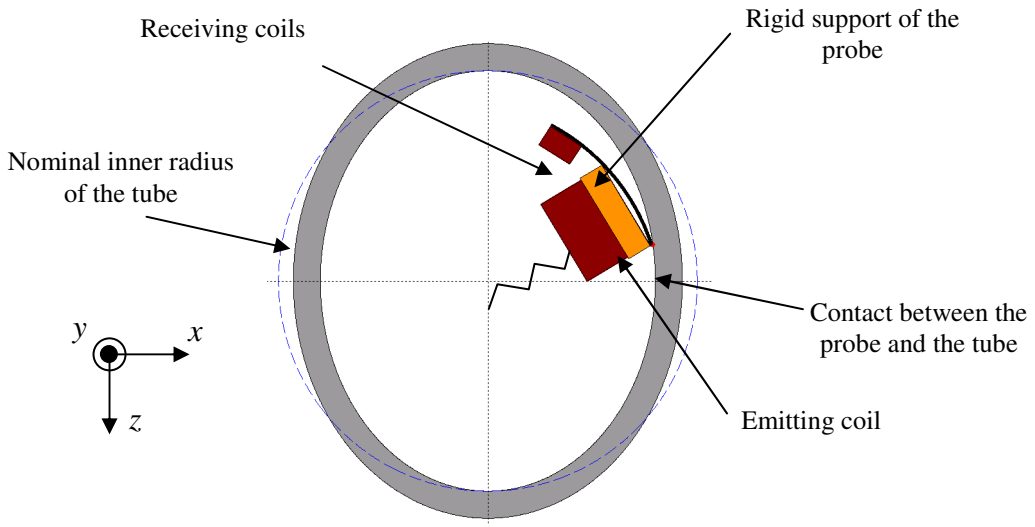


Figure 7 - Example of ECT configuration involving a rotating probe in a SG tube with an out-of-roundness different from 0. Different lift-offs appear for each coil, despite the presence of the spring.

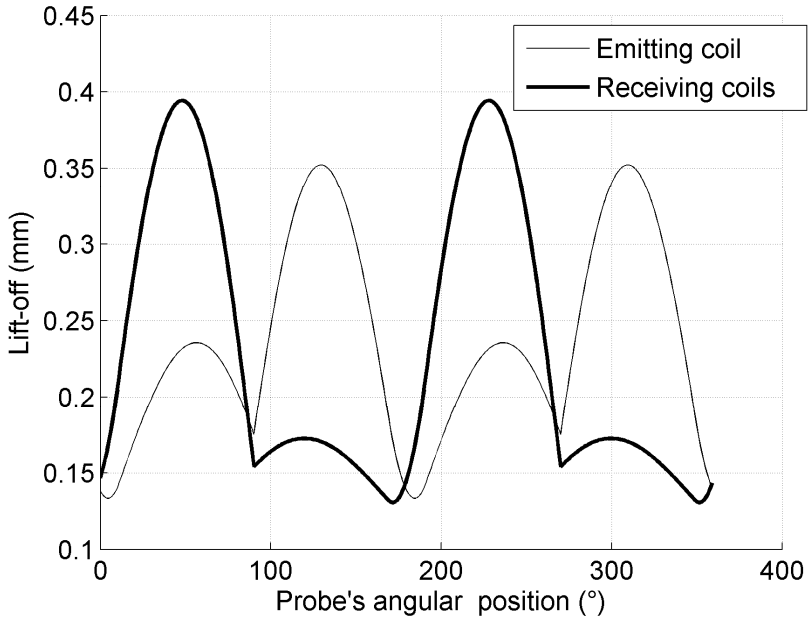


Figure 8 - Plot of each coil's lift-off versus the probe's angular position, for a SG tube with a relative out-of-roundness of 4%.

As models developed at CEA cannot up to now take into account a lift-off variation with the probe's angular position, several cartographies were simulated with constant lift-off values corresponding to some positions, detailed in table 3, and maximal variations □Y were calculated (see previous section). Moreover, estimations of cartographies taking into account a lift-off-variation with the probe's angular position were calculated as weighted sums of these cartographies.

| Angular position | 0° | 25° | 50° | 75° | 90° | 105° | 130° | 155° |
|---|---|---|---|---|---|---|---|---|
| Lift-off of the emitting coil (mm) | 0.13 | 0.18 | 0.23 | 0.23 | 0.18 | 0.28 | 0.35 | 0.28 |
| Lift-off of receiving coils (mm) | 0.13 | 0.32 | 0.39 | 0.28 | 0.15 | 0.17 | 0.17 | 0.15 |

Table 3 - Couples of lift-off values used in simulation

## NEW TOOLS AVAILABLE IN CIVA FOR PARAMETRIC STUDIES

New tools dedicated to the management of simulations results and the study of parameters variation have been added in the release 9 of the CIVA platform. These tools provide the possibility to compare simulations with respect to a reference, to generate a HTML report for each calculation, and to plot directly the evolution of the result, like the maximal amplitude of a 1D ECT signal for instance, with respect to variations of some configuration's parameters. An example of a parametric study is shown in figure 9. In this case, the configuration addresses a SG tube tested with the bobbin coil described previously in this article. Flaws considered in this set of simulations are internal longitudinal notches with a length of 3 mm and an opening of 10°. Their depths vary from 10% of the tube's thickness (i.e. 0.127 mm) to 100%. This ECT configuration has been defined only once in the CIVA user interface and, given the range of the parameter variation (i.e. the flaw depth in this example), all calculations are automatically run in a background task. It is afterwards possible to plot the effect of the variation with respect to the corresponding parameter. In figure 9, one can see the effect of the flaw's depth on the maximal amplitude and the phase in the complex plane (see figure 1) of the ECT signal, when considering a scan of the probe along the tube's axis.

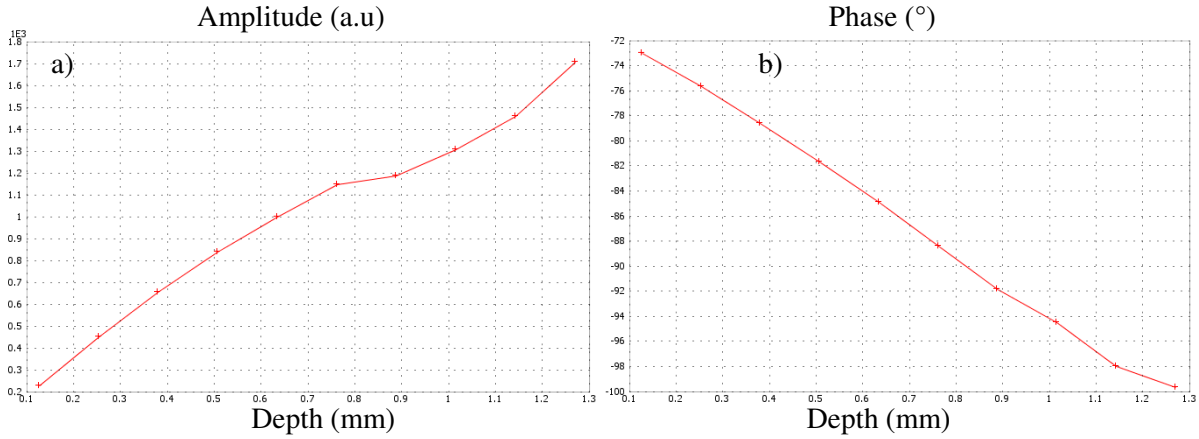


Figure 9 - Effect of the depth's variation of the flaw on a) the simulated signal's maximal amplitude and b) on its phase, respectively, In the case of an axial probe testing a SG tube at 500 kHz. The flaw's depth varies from 10% (i.e. 0.127 mm) to 100%.

## CONCLUSIONS

This paper has presented recent progresses in developing models dedicated to steam generator tubing inspection. These codes, integrated in the CIVA platform, are based on semi-analytical approach to obtain fast and accurate results. Representative configurations of bobbin coil and rotating probe inspections were illustrated, and results obtained show the good agreement between experimental and simulated data.

These models are helpful to study various ECT configurations, but are also particularly useful to assess the impact of perturbation parameters by limiting the number of experimental tests. Thus, the examples illustrated in the article show the influence on the detection performances of the bobbin coil eccentricity, the coils positioning and the geometry variation for the rotating probe inspection.

## REFERENCES


1) Chew W.C, *Waves and Fields in Inhomogeneous Media*, Piscataway, IEEE Press (2nd edition), 1995.
2) Prémel D, Pichenot G and Sollier T, "Development of a 3D electromagnetic model for eddy current tubing inspection", *International Journal of Applied Electromagnetics and Mechanics*, 2004 19 521-525.
3) Harrington R.F, "The Method of Moments in Electromagnetics", *Journal of Electromagnetic Waves and Applications*, 1987 1 (3) 181–200.
4) Reboud C, Prémel D, Pichenot G, Lesselier D and Bisiaux B, "Development and validation of a 3D model dedicated to eddy current non destructive testing of tubes by encircling probes", *International Journal of Applied Electromagnetics and Mechanics*, 2007 25 313-317.
5) Auld B.A and Muennemann F.G and Riaziat M, *Nondestructive testing, Chapter 2: Quantitative modelling of flaw responses in eddy current testing*. vol. 7, London, Academic Press, 1984.